

Identification and investigation of martian dust source regions from orbital observation

Laura Kulowski,¹ Huiqun Wang²

Abstract.

We have constructed a database of locations of active dust lifting on Mars from existing Mars Daily Global Maps (MDGMs). The daily global maps used in this study were generated from wide-angle images taken by the Mars Orbiter Camera (MOC) on Mars Global Surveyor (MGS) (Mars Years 24-27, July of 1999 to January of 2005). We have concentrated on the “equatorial map” (60° N- 60° S) and the periods without global dust storms in this paper. Areas of active dust lifting in each MDGM were visually identified based on an analysis of albedo changes, color, and morphology. Using this database, we assess the spatial, temporal, and size distribution of lifting areas and classify lifting events by structure. Lifting is found to be concentrated in three seasonal windows: $L_s = 0^{\circ}$ - 80° , $L_s = 130^{\circ}$ - 230° , and $L_s = 260^{\circ}$ - 360° . Large-scale lifting mainly occurs in the $L_s = 130^{\circ}$ - 230° seasonal window. Northern and southern lifting events also have preferred seasonal windows of occurrence, with northern ones concentrated during $L_s = 180^{\circ}$ - 230° and $L_s = 280^{\circ}$ - 360° and southern ones concentrated during $L_s = 20^{\circ}$ - 60° and $L_s = 130^{\circ}$ - 220° . Both annually and for the identified seasonal windows, the number of small lifting events far exceeds the number of large ones. Observations indicate that active dust lifting is most frequently observed in the Arcadia, Acidalia, Argyre, and Hellas regions while inactive regions include Tharsis, Arabia Terra, and sections of Elysium. These locations correspond well with GCM predicted annual surface wind stress and dust deposition distributions. In this paper, three morphological categories for active dust lifting are defined: puffy, pebbled, and plume. We demonstrate that these structures are apparent in all seasonal windows. Our data also suggests that pebbled and plume morphologies occur at similar latitudes and times of the year. Puffy structures are differentiated from pebbled and plume structures in that they occur more frequently at lower latitudes.

1. Introduction

Following observations of “yellow clouds” by French astronomer *H. Flaugergues* [1818] and Italian astronomer *G. V. Schiaparelli* [1895], Mars became famed for its dust storm activity. With the realization of spacecraft observations during the 1970s, scientists received detailed images of Martian dust events. Mariner 9 captured the decay phase of the 1971 global dust storm [Leovy *et al.*, 1972]. The orbiter also witnessed local dust storms along the edge of the northern polar cap during the extended phase of the mission. Further observations were made by the Viking missions between 1976 and 1979. Since 1999, Mars Global Surveyor (MGS) and Mars Reconnaissance Orbiter (MRO) have provided scientists with the longest systematic daily global record of Martian weather.

Dust activity on Mars ranges from dust devils spanning a few square meters to planet scale global dust storms. Historically, the classification of dust storms has varied between observers. Non-local dust storms, including regional and planet-encircling dust storms, were classified by *Martin and Zurek* [1993] as storms with the long axis greater than 2,000 km. *Cantor et al.* [2001] extended *Martin and Zurek's* [1993] definition by specifying regional dust storms as those with

Table 1. Martian Seasons

L_s	Northern Season	Southern Season	Length (days)
0° - 90°	Spring	Fall	199
90° - 180°	Summer	Winter	183
180° - 270°	Fall	Spring	147
270° - 360°	Winter	Summer	154

areas greater than $1.6 \times 10^6 \text{ km}^2$ and persisting for more than 3 sols (where one sol is 24h 39m 35s). *Wang and Richardson* [2013] also altered the definition by designating large dust storms as those influencing multiple regions on Mars and persisting for more than 5 sols. Since dust devils are beyond the resolution of the data we analyze (Section 2), this paper concentrates on lifting associated with dust storms.

Martian dust storms are complex phenomena that vary in time, location, size, and severity. Seasonal dates on Mars are conveniently defined in terms of areocentric longitude, L_s . Areocentric longitude refers to the position of the planet with respect to the Sun, with $L_s = 0^{\circ}$ defined as the northern spring equinox (see Table 1). Small, local-scale dust storms are apparent throughout the year [*Cantor*, 2007]. Regional storms are yearly events and occur during preferred seasonal windows, such as $L_s = 210^{\circ}$ - 240° and $L_s = 310^{\circ}$ - 340° [*Hinson and Wang*, 2010; *Smith*, 2008; *Wang*, 2007]. Major dust storms, which last for several weeks or months, occur mainly during the southern spring and summer, which is conventionally referred to as the “dust storm season.” During this time of the year, the planet is near its perihelion and has the warmest atmospheric and surface temperatures. The most fantastic storm activity on the planet is when these large storms develop into global scale storms. Planet engulfing

¹Department of Mathematics, Brown University, Providence, Rhode Island, USA.

²Atomic and Molecular Physics Division, Harvard-Smithsonian Center for Astrophysics, Cambridge, Massachusetts, USA.

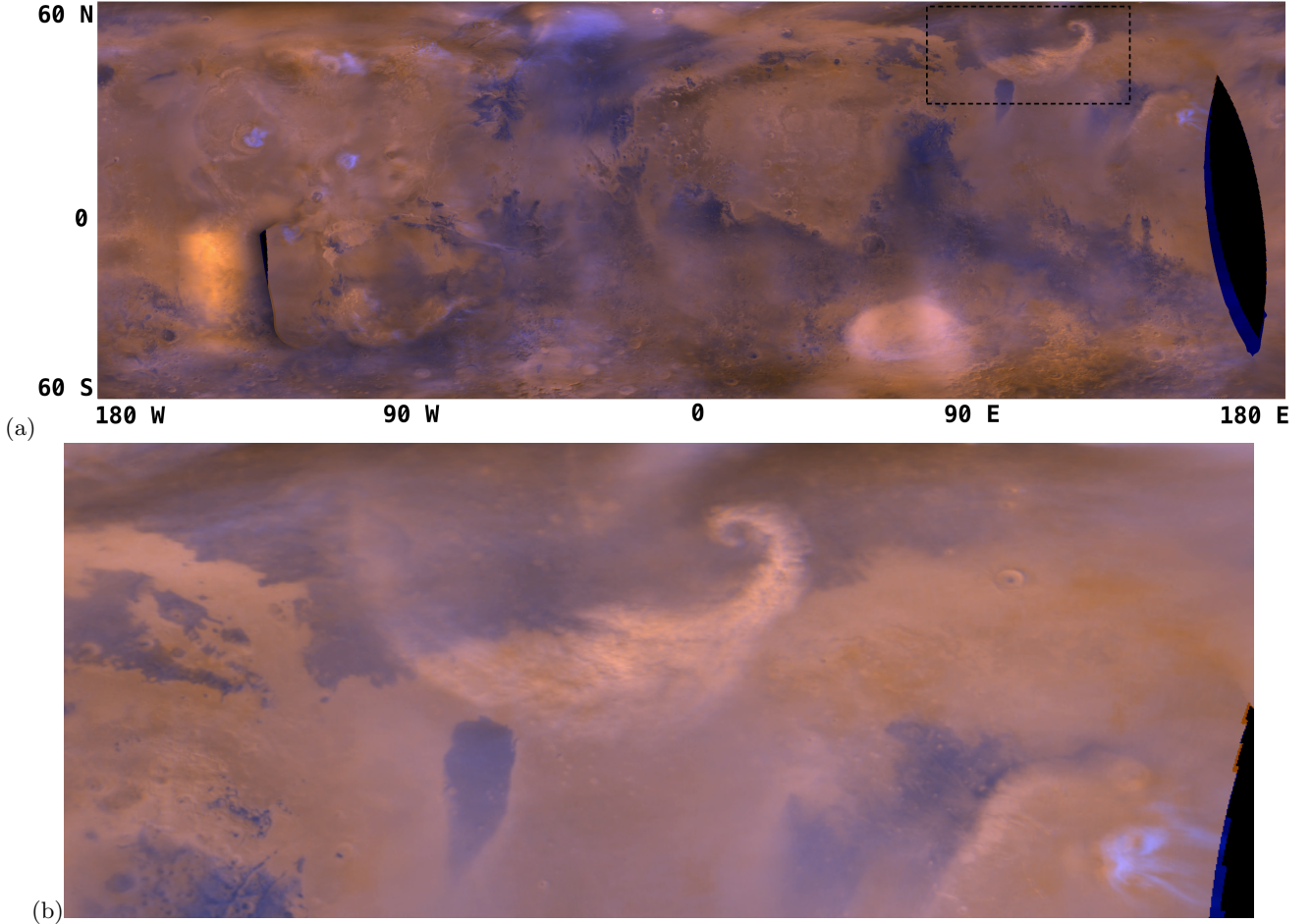


Figure 1. A MGS/MOC MDGM at $L_s=13.5^\circ$ with an area of active lifting included in boxed region. Note that the blue and black patches in the lower right region of the map are due to missing data. (b) A zoomed in view of the lifting event associated with a curvi-linear shaped weather front. The plume-like structure along the front indicates fresh dust lifting.

storms are not annual events, but occur at random intervals every few Martian years. However, during the opposite season ($L_s = 0^\circ\text{--}180^\circ$), the global mean optical depth of dust decreases dramatically, storms becomes less frequent, and the climate is highly repeatable in terms of global mean air temperature and dust opacity [Liu *et al.*, 2003].

Although our understanding of Mars has improved in recent years, we still have much to learn about the mechanics behind the origins of dust storms. Several dust lifting schemes have been suggested from observations and theoretical calculations. Greeley *et al.* [1980] found that direct lifting of dust particles between 10–100 μm requires surface winds in excess of 30 m s^{-1} . Other proposed mechanisms for dust lifting include saltation and dust devils. Saltation is a process during which large particles lifted into the atmosphere travel short distances. Upon impact with the ground, these particles lift secondary, finer grain particles. This process repeats itself, resulting in positive feedback and dust lifting. Unlike saltation, vortex wind speed associated with dust devils is independent of particle size [Greeley *et al.*, 1980; Neubauer, 1966]. Once airborne by surface winds, saltation, or dust devils, these dust particles may be transported and mixed by atmospheric circulation (planetary boundary layer turbulent mixing, zonal mean circulation, and eddies) to form dust storms of various morphologies.

While prior studies (e.g., Cantor *et al.*, 2001; Wang and Richardson, 2013) have summarized locations of dust storms observed in images, an analysis that highlights the regions

of active dust lifting has not yet been carried out. Such an analysis is important for several reasons. It makes sense to first ground our understanding of Martian dust lifting on actual lifting events rather than those predicted by models. Analyses can be made on the spatial and temporal distribution of lifting, allowing us to put constraints on the Martian dust cycle. This, in turn, leads to a better understanding of the Martian surface-atmosphere system and climate. From our analysis, we can derive occurrence frequency maps of active dust lifting. These maps allow us to infer how surface properties (dust abundance, topography, roughness) and near surface meteorology work together to control lifting events. The frequency, seasonality, size, and structure of lifting phenomena included in this database can be used to validate predictions of numerical simulations or be used in data assimilation to improve model performance.

This paper presents the results of surveying the Mars Daily Global Maps (MDGM) composed using Mars Global Surveyor's (MGS) Mars Orbiter Camera (MOC) for locations of active dust lifting. We begin by describing our visual identification method. The remaining sections discuss the temporal, spatial, and size distribution of active dust lifting, the frequency of dust lifting with attention to surface properties and GCM predicted wind stress and dust deposition patterns, and the distribution of various lifting structures.

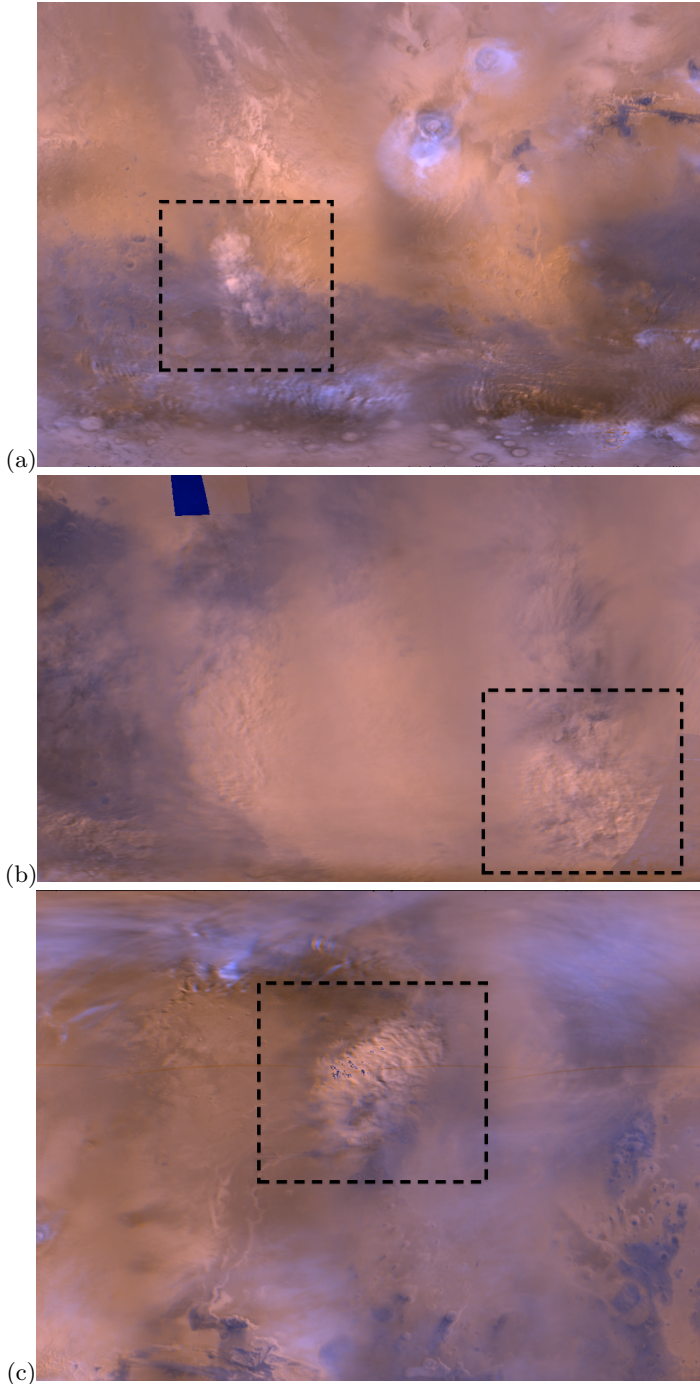


Figure 2. Three examples of active dust lifting are enclosed in dashed boxes. Note the different morphology features of each lifting site. Lifting in panel (a) has a puffy structure, lifting in panel (b) has a pebbled, grainy structure, and panel (c) has a plume-like structure.

2. Analysis Techniques

2.1. Instrument

The data sets used in this study are the Mars Daily Global Map (MDGM) archive, which is composed of wide-angle images from the Mars Orbiter Camera (MOC) on board the Mars Global Surveyor (MGS) [Wang and Ingersoll, 2002]. To gain an understanding of “normal” conditions, we have excluded the Mars Year 25 global dust storm

($L_s = 185^\circ$ - 263°) from this study. The detailed development history of this global dust storm is described by Strausberg *et al.* [2005] and Cantor [2007].

MGS operated in a polar orbit around the planet with a 1.95 h period. On MGS, MOC was pointed at nadir and equipped with one narrow-angle camera and two wide-angle cameras. One wide-angle camera used a red filter (575-625 nm) while the other wide-angle camera used a blue filter (400-450 nm). From an average height of 378 km from the surface, MOC captured images of the planet at a nominal 7.5 km pixel⁻¹ resolution. Approximately every 24 hours,

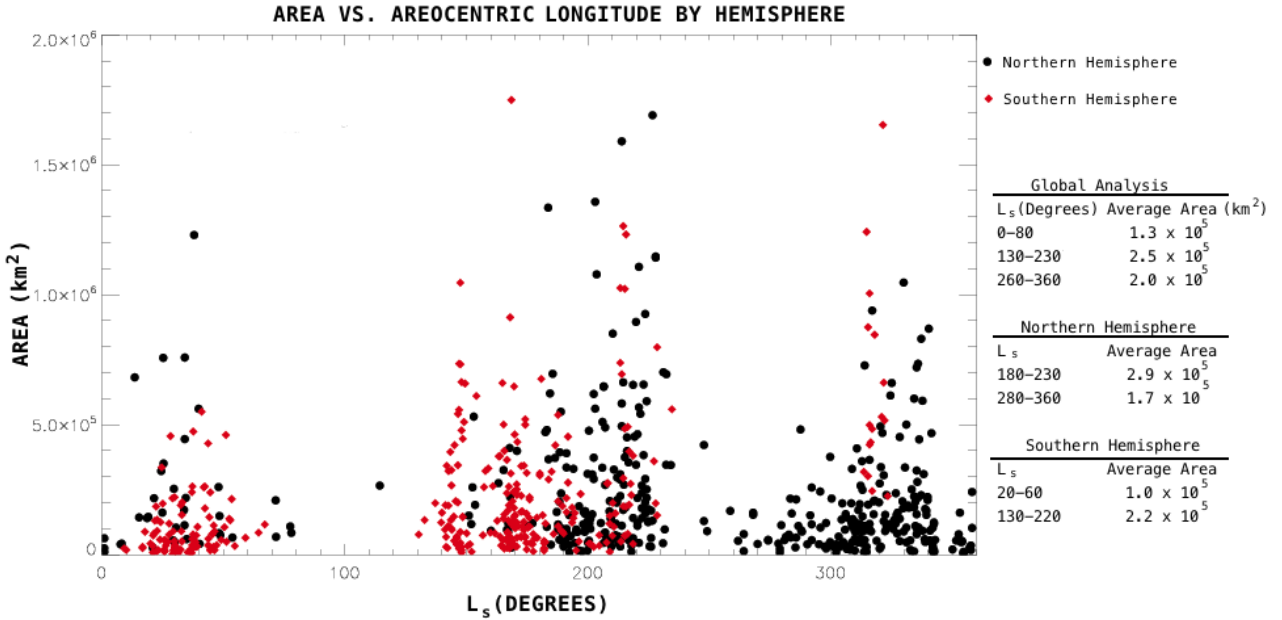


Figure 3. Area of each lifting event as a function of areocentric longitude for July of 1999 to January of 2005. Data points are grouped into northern lifting events (black) and southern lifting events (red).

MGS/MOC took between twelve to thirteen sets of pole-to-pole and limb-to-limb image swaths in the red and blue wavelengths to generate a complete daily view of Mars. These swaths were combined to create a Mars Daily Global Map (MDGM). Using our color scheme, dust storms have an orange or red appearance while condensate clouds are blue or white in MDGMs.

2.2. Daily Global Maps

Each MDGM has a spatial resolution of 0.1×0.1 degree so dust activity larger than tens of kilometers can be visually identified. Our method to identify areas of active dust lifting comprises four steps. First, consecutive MDGMs are examined for albedo variations associated with dust storms and clouds. Second, we examine maps that show albedo variations for dust storms based on color. Third, regions identified as dust storms are scrutinized more closely for structures associated with active dust lifting, such as convective dust lobes and the appearance of pebbled or plume-like fine-scale dust structures (Figure 1). Finally, once an area of active dust lifting is identified, it is manually marked in the MDGM and stored in an object containing information about the location, size, time, and morphology of the identified dust lifting event. We have devised three morphological classifications, puffy, pebbled, and plume, to describe the variety of morphologies observed in MDGMs (Figure 2). Puffy morphologies characterize inflated, turbulent structure. Pebbled morphologies characterize granular structure and plume morphologies characterize collimated structure. From this collection of data, we study the spatial, temporal, and size distribution of lifting, derive dust lifting frequency maps, and examine the patterns of lifting morphologies.

It should be noted, however, that a MDGM does not represent a snapshot of the whole planet. Instead, a map gives us a view of the planet gradually being built up throughout the course of a day. MGS/MOC made its observations at about 2PM local time, thus limiting our results to be at this particular time. Additionally, we have only examined the equatorial maps, which extend in latitude from 60°N to 60°S . Despite these limitations, the observations made by MGS/MOC are one of the most complete records of the planet and can provide strong constraints for numerical models.

3. Analysis

3.1. Active Dust Lifting Size Distributions

The MGS/MOC MDGM is in simple cylindrical projection and each pixel has its own pre-defined area. Using the Interactive Data Language (IDL), we were able to visually inspect the Martian surface for regions of fresh lifting events. The total area of all the pixels within the identified lifting area is calculated as the area of the corresponding lifting event. In this section, we discuss how the area of fresh lifting in our database varies with the time of year for both the planet as a whole and then for each hemisphere.

3.1.1. Global Analysis

In total, we obtained 769 dust lifting events between July of 1999 and January of 2005, excluding the 2001 global dust storm. The areas ranged from a Connecticut-sized lifting event of $1.57 \times 10^3 \text{ km}^2$ to an Alaska-sized lifting event of $1.87 \times 10^6 \text{ km}^2$.

Figure 3 shows the area of the events as a function of areocentric longitude. A trend in the time of year at which dust lifting occurs and size of the dust lifting event is apparent. Lifting tends to occur in three seasonal windows. The first seasonal window takes place during $L_s = 0^\circ-80^\circ$. After a period of inactivity, dust lifting recommences during $L_s = 130^\circ-230^\circ$. The third period of lifting takes place during $L_s = 260^\circ-360^\circ$. The latter two seasonal windows overlap with the traditional dust storm season. The average area of lifting are $1.3 \times 10^5 \text{ km}^2$, $2.5 \times 10^5 \text{ km}^2$, and $2.0 \times 10^5 \text{ km}^2$, respectively, for the three seasonal windows.

Figure 3 clearly shows that small lifting events are much more common than large lifting events. In order to obtain a more detailed understanding of the annual size distribution of active dust lifting on Mars, we have plotted a histogram in Figure 4a. The number of lifting events drastically decreases as the surface area increases. We have counted 564 instances of active dust lifting with surface areas less than $2.5 \times 10^5 \text{ km}^2$, 124 events between $2.5 \times 10^5-5.0 \times 10^5 \text{ km}^2$, which is a factor of 4.5 less, and 50 events between $5.0 \times 10^5-7.5 \times 10^5 \text{ km}^2$, which is a factor of 2.5 less than the previous category. The largest bin between $1.5 \times 10^6-1.75 \times 10^6 \text{ km}^2$ only contains 4 events. Figure 5 shows the logarithm

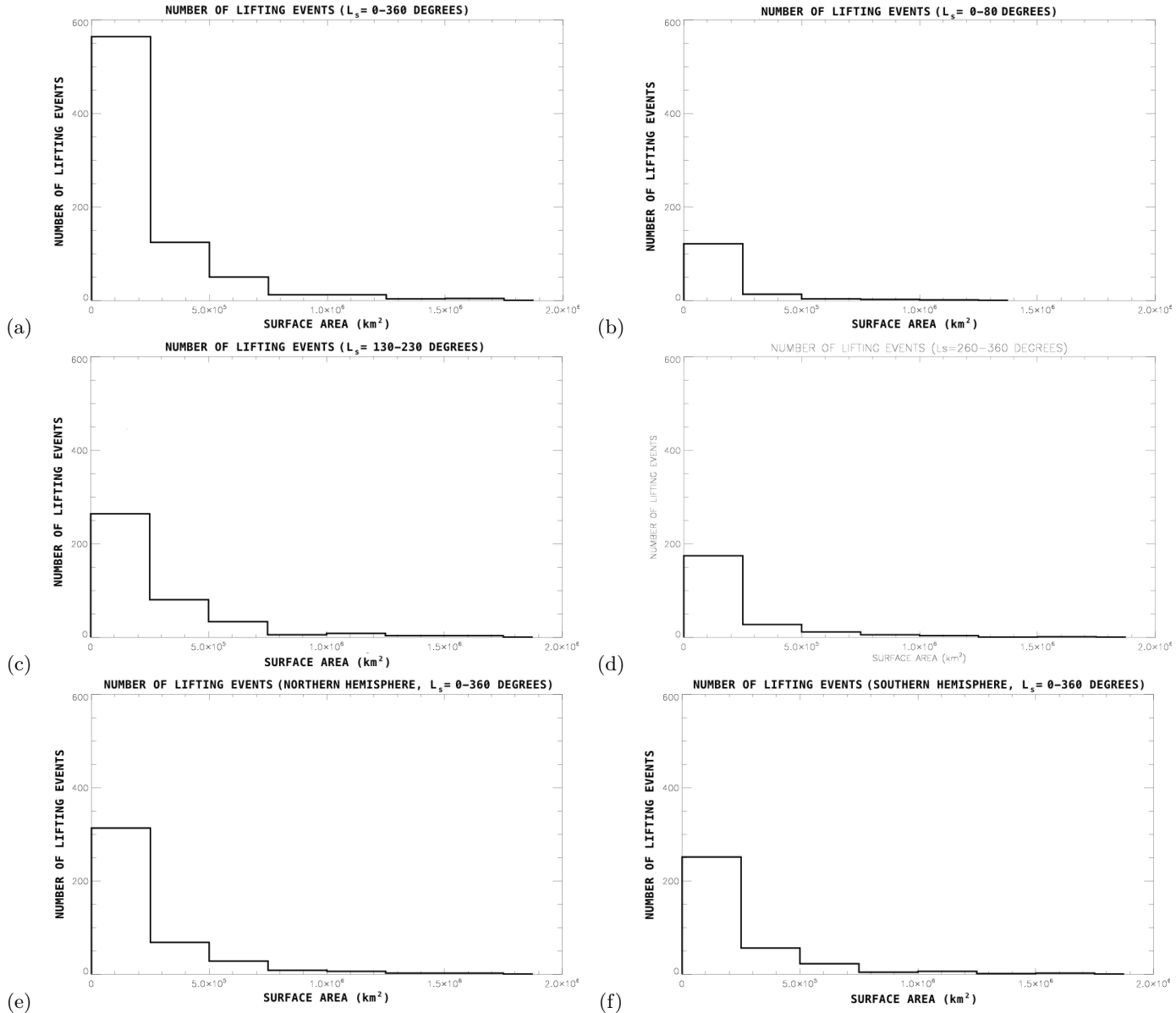


Figure 4. Histograms of the number of lifting events as a function of surface area for the entire Martian year, three seasonal bins, and each hemisphere. For all time scales, lifting activity is dominated by sources with areas less than 2.5×10^5 km². Small lifting activity is also dominant on both global and hemispheric scales.

of the number of lifting events as a function of each area bin. An exponential best fit with a slope of -1.47×10^{-6} describes the decay rate. The rapid decay of the number of events with increasing area is observed for all seasonal windows, although the details associated with each seasonal window differ (see Figure 5). Note that the first seasonal window, which occurs outside of the dusty season, has the most severe decay rate.

Figure 4b-d shows the histogram for the three seasonal windows previously identified. Apparently, the period of the greatest number of lifting events occurs during the second seasonal window ($L_s = 130^\circ\text{--}230^\circ$) and the least number of lifting events during the first seasonal window ($L_s = 0^\circ\text{--}80^\circ$). The 264 lifting events with areas less than 2.5×10^5 km² recorded for the second seasonal window is more than double the 121 events recorded for this area grouping during the first seasonal window. The second seasonal window also has a greater number of events with large surface areas. During the first seasonal window, only one lifting source has an area between $1.0 \times 10^6\text{--}1.25 \times 10^6$ km². During the third

seasonal window, 3 lifting source has an area between $1.0 \times 10^6\text{--}1.25 \times 10^6$ km² and one lifting event has an area between $1.5 \times 10^6\text{--}1.75^6$ km². The second seasonal window boasts 8 events with areas between $1.0 \times 10^6\text{--}1.25^6$ km², 3 events with areas between $1.25 \times 10^6\text{--}1.5^6$ km², and 3 events with areas between $1.5 \times 10^6\text{--}1.75^6$ km². The trend shown in Figures 4b-d is also indicated in Figure 3.

3.1.2. Hemispheric Analysis

The northern and southern hemispheres of Mars are remarkably different. On average, there is a 5 km difference in elevation between the lower north and the higher south. Unlike the younger and smoother northern hemisphere, the crust of the southern hemisphere is heavily cratered. The asymmetry between the northern and southern hemispheres motivates our desire to examine our results by separating events in the northern hemisphere from events in the southern hemisphere.

In Figure 3, black circles represent northern events and red diamonds represent southern events. The northern and

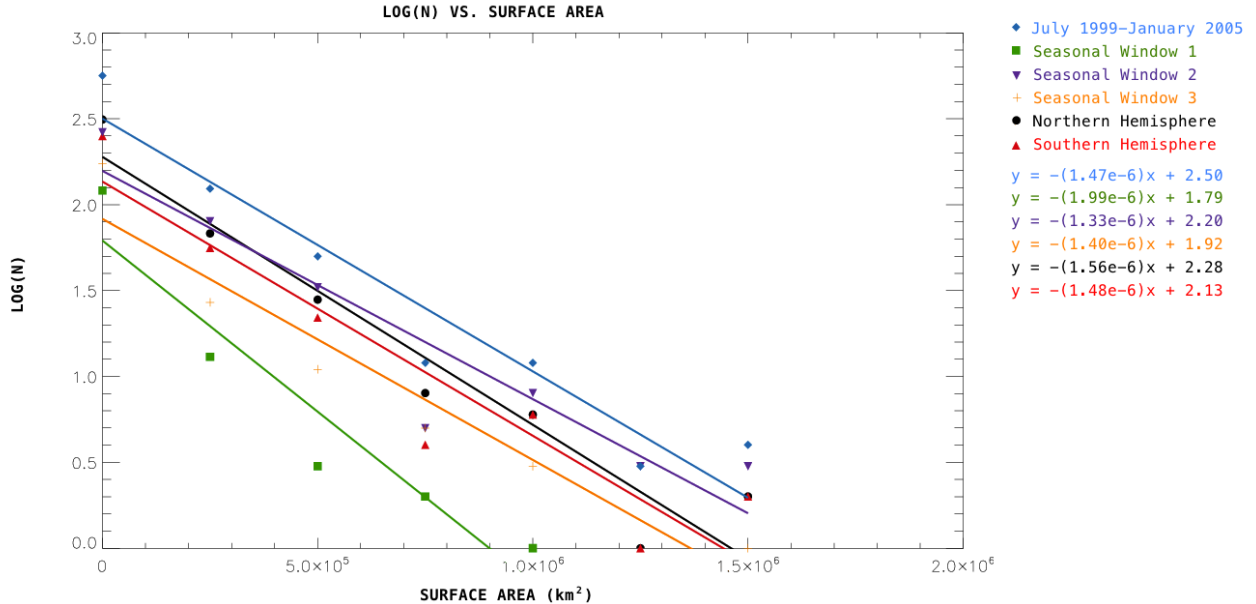


Figure 5. Logarithm of the number of lifting events, N, as a function of size. Solid best fit lines and their corresponding equations are shown.

southern events each have their own preferred seasonal windows of occurrence. Northern ones are more concentrated during $L_s = 180^\circ\text{--}230^\circ$ and $L_s = 280^\circ\text{--}360^\circ$, with fewer lifting events during $L_s = 0^\circ\text{--}80^\circ$. The average area of lifting is $2.9 \times 10^5 \text{ km}^2$ and $1.7 \times 10^5 \text{ km}^2$, respectively, for these two time periods. Southern events are more concentrated during $L_s = 20^\circ\text{--}60^\circ$ and $L_s = 130^\circ\text{--}220^\circ$ with average lifting areas of $1.0 \times 10^5 \text{ km}^2$ and $2.2 \times 10^5 \text{ km}^2$, respectively. It should be noted that these results are for $60^\circ\text{N}\text{--}60^\circ\text{S}$. We have not considered the high latitude areas in this study.

Figures 4e-f show that northern and southern populations exhibit the usual trend of rapid decay in number of lifting events as the surface area increases. The rate of decay is similar for each hemisphere. We counted 313 events in the north with areas less than $2.5 \times 10^5 \text{ km}^2$, 68 events with areas between $5.0 \times 10^5 \text{ km}^2\text{--}7.5 \times 10^5 \text{ km}^2$ (about 4.6 times less than the previous category), and 28 events with areas between $2.5 \times 10^5 \text{ km}^2\text{--}5.0 \times 10^5 \text{ km}^2$ (about 2.4 times less than the previous category). For the south, we recorded 251 events with areas less than $2.5 \times 10^5 \text{ km}^2$, 56 events with areas between $5.0 \times 10^5 \text{ km}^2\text{--}7.5 \times 10^5 \text{ km}^2$ (about 4.5 times less than the previous category), and 22 events with areas between $2.5 \times 10^5 \text{ km}^2\text{--}5.0 \times 10^5 \text{ km}^2$ (about 2.5 times less than the previous category). Figure 5 gives the best fit slopes for the decay in the number of lifting events as surface area increases as -1.56×10^{-6} in the northern hemisphere and -1.48×10^{-6} in the southern hemisphere.

4. Active Dust Frequency Distributions

The Martian dust cycle consists of lifting, transport/mixing, and deposition. Dust supply is one factor affecting lifting, but surface wind stress and convection are also important factors. Here, we analyze the frequency of dust lifting over different time scales and compare our results to surface properties (topography, surface albedo, and thermal inertia) and GCM simulations.

Figure 6a shows the frequency of lifting for all of the events in our database. The frequency for each pixel is calculated as the number of days with lifting divided by the total 1591 days we have examined. It is apparent that dust

lifting is non-uniformly distributed across the planet. We can divide lifting areas into three groups: the northern mid-latitude band, the low latitude population, and the southern mid-latitude band. The northern mid-latitude band contains several regions with the highest dust lifting frequencies, including the Arcadia and Acidalia regions. The low latitude population is highly asymmetric in zonal distribution. Lifting is concentrated in low topographic channels, especially in Chryse and western Elysium Planitia in the northern low latitudes. Limited zonal expansion is observed in the southern low latitudes, though the lifting frequency is far less than that in the north. The southern mid-band exhibits more zonal symmetry than the other two groupings. High frequency lifting areas are in Hellas and Argyre.

A few broad observations can be made when comparing Figure 6a with Mars topography, albedo and thermal inertia maps. The high frequency northern lifting sites (Arcadia and Acidalia) have low elevations and flat, smooth topography. High frequency southern lifting sites (Hellas and Argyre) are large impact basins on the southern highland. Inactive regions include Tharsis, Arabia Terra, and large sections in Elysium Mons area. These areas have overall higher topography and lower thermal inertia than the surrounding. However, no simple correlation is evident on a global scale.

Current GCMs parameterize dust lifting according to two mechanisms: dust devil lifting (presumably related to convective cells) and surface wind stress lifting. Our data set pertains to the wind stress lifting mechanism. It is therefore useful to compare our observations with predictions of models. Basu *et al.* [2006] and Mulholland *et al.* [2013] provided plots of annual maximum surface wind stress predicted by two different GCMs. Both predict high wind stress in Arcadia, Acidalia, and Hellas. These locations correspond well with our high frequency lifting areas. The models also suggest that Tharsis, Arabia, and Elysium are net dust deposition areas and our results show no active lifting in these regions. There are a few discrepancies, however. Basu *et al.* [2006] found that the Syria region was characterized by

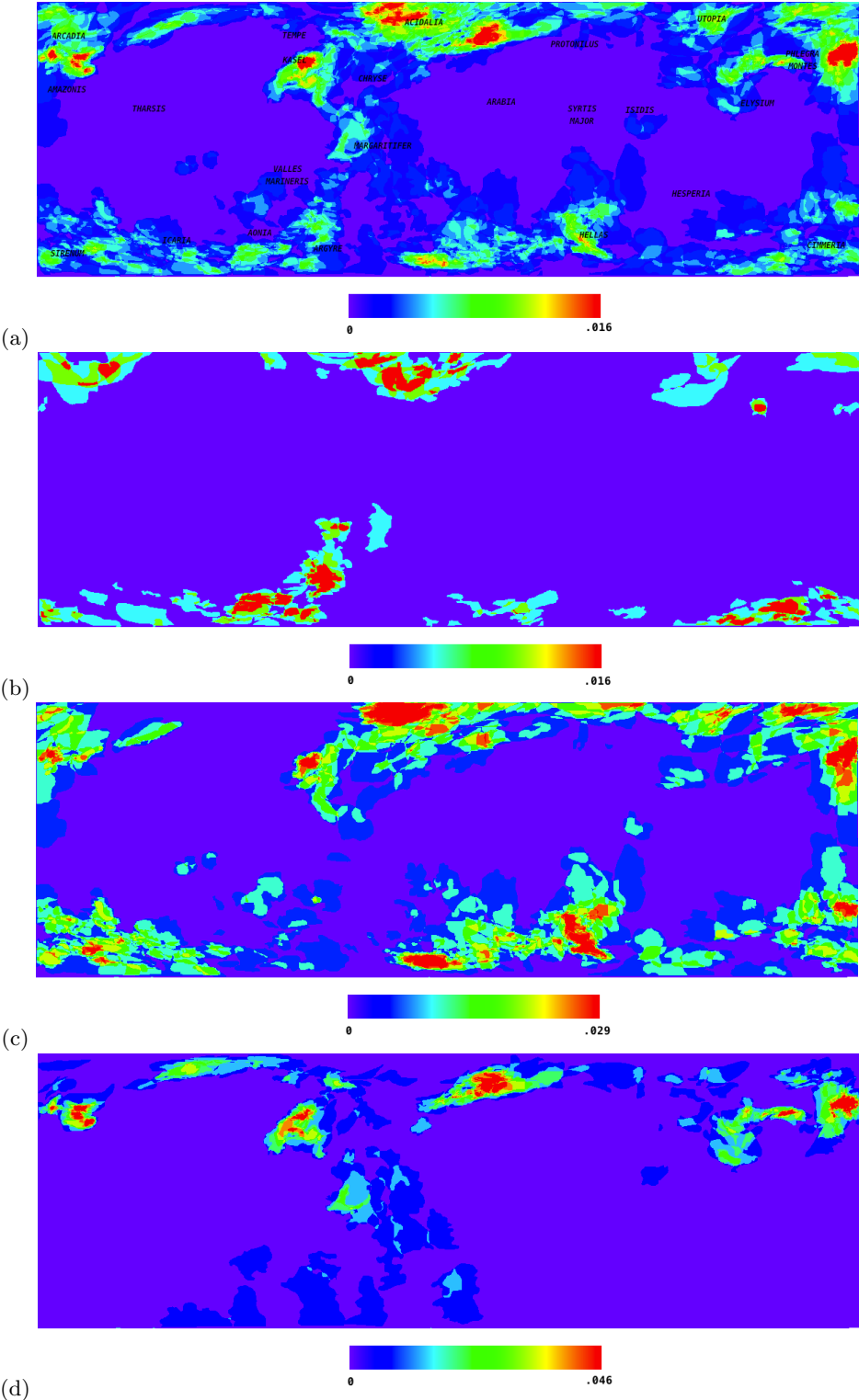


Figure 6. Frequency of lifting events for (a) July of 1999 to January of 2005, (b) $L_s = 0^\circ\text{-}80^\circ$, (c) $L_s = 130^\circ\text{-}230^\circ$, and (d) $L_s = 260^\circ\text{-}360^\circ$. In this context, frequency refers to the number of days with lifting within the period considered divided by the total number of days within the period for each pixel.

weak surface stress and that it did not contribute to dust storms in their simulations. Our results show that lifting is apparent in this region. GCM models predict high wind stress in Protonilus and Utopia. Figure 6a shows these areas did not have maximum lifting frequencies. It should be noted that our results are limited to approximately 2PM

local time, while the GCM results are not. We have only worked on data for Mars Year 24-27, while more data are needed to get better statistics. GCM results are sensitive to resolution and dust scenarios. Physics parameterization may still need to be improved.

In Figures 6b-d, we have generated the frequency maps for the three seasonal windows identified in the previous sec-

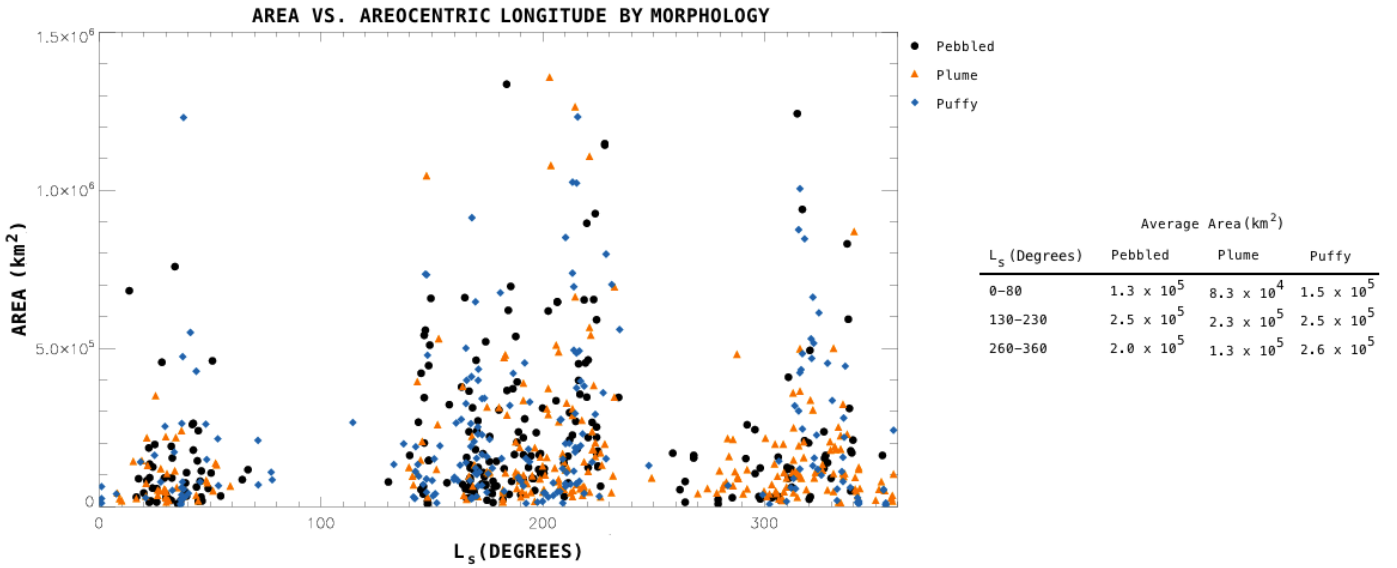


Figure 7. Area of each lifting event as a function of areocentric longitude for July of 1999 to January of 2005. Data points are grouped into puffy, pebbled, and plume morphological categories. All morphologies are observed in all seasonal windows.

tion ($L_s = 0^\circ\text{-}80^\circ$, $L_s = 130^\circ\text{-}230^\circ$, and $L_s = 260^\circ\text{-}360^\circ$). Each one is calculated with respect to the total number of days within the seasonal window. During the first seasonal window, the northern mid-latitude band and the southern mid-latitude band are active and the low latitude population was relatively inactive. Areas of high frequency dust lifting include the Arcadia, Acidalia, and Elysium regions in the north and the Aouia and Cimmeria regions in the south. Lifting in the low latitude is concentrated in the Valles Marineris.

The second seasonal window is the most active period of dust lifting. Lifting is apparent in all three lifting groups, although the northern and southern mid-latitude bands are more active than the low latitude population. Most northern lifting is concentrated in the Acidalia and Arcadia regions. High frequency lifting sites in the north are the largest in zonal coverage, with the most expansive one in the Acidalia. Low latitude lifting occurs in Chryse and sections of Elysium and Amazonis. During the second seasonal window, the Hellas basin became active. Overall, southern activity has greater zonal symmetry than the northern band or the low latitude population.

During the third seasonal window, the northern mid-latitude band is similar to that in the second seasonal window. The low latitude population show much southward extension and the south is much less active. Hellas is no longer a source of active dust lifting. Lifting occurs in Icaria, Aonia, and Argyre, which appear to be extensions from the low latitude population.

4.1. Morphological Properties of Active Dust Lifting

As mentioned earlier, we define three morphological categories for dust lifting structures. Our first group contains puffy, convective structures, our second group contains pebbled, grainy structures, and our third category contains plume-like structures (Figure 2). The purpose of this section is to relate morphology to season, surface area of the

lifting event, and location on the planet. Only events clearly identified as puffy, plume, or pebbled lifting (91 percent of our data) are considered. Ambiguous cases and cases with multiple morphologies are ignored in this analysis.

4.1.1. Seasonal Variations

Figure 7 shows the area of lifting events plotted as a function of areocentric longitude for each morphological category. Puffy, pebbled, and plume structures show no seasonal preference and are apparent in all the seasonal windows defined in Section 3.2 ($L_s = 0^\circ\text{-}80^\circ$, $L_s = 130^\circ\text{-}230^\circ$, and $L_s = 260^\circ\text{-}360^\circ$).

The structure of a lifting region seems to be related to the overall size of the event. In particular, puffy and pebbled morphologies tend to be larger than plume morphologies. The average area for puffy structures is $1.5 \times 10^5 \text{ km}^2$, $2.5 \times 10^5 \text{ km}^2$, and $2.6 \times 10^5 \text{ km}^2$, respectively, for the three seasonal windows. The average area for pebbled structures is $1.3 \times 10^5 \text{ km}^2$, $2.5 \times 10^5 \text{ km}^2$, $2.0 \times 10^5 \text{ km}^2$, respectively, which is quite similar to that of the puffy structures. Plume morphologies have an average area of $2.3 \times 10^5 \text{ km}^2$ during the second seasonal window, which is similar to that for pebbled and puffy morphologies for this time period. However, during the first and third seasonal window plume structures have average areas of $8.3 \times 10^4 \text{ km}^2$ and $1.3 \times 10^5 \text{ km}^2$, respectively. These values are significantly smaller than those for pebbled and puffy morphologies.

4.1.2. Latitudinal Distribution

A comparison of the latitudinal versus areocentric longitude distribution of the three identified morphologies is shown in Figure 8. In this plot, the size of each symbol is proportional to the area of the lifting event. Several observations can be made. It is apparent that the dust lifting is more common at higher latitudes, in accordance with Figure 3. About 86 percent of lifting events take place above 30° N/S , 59 percent take place above 40° N/S , and 29 percent occur above 50° N/S .

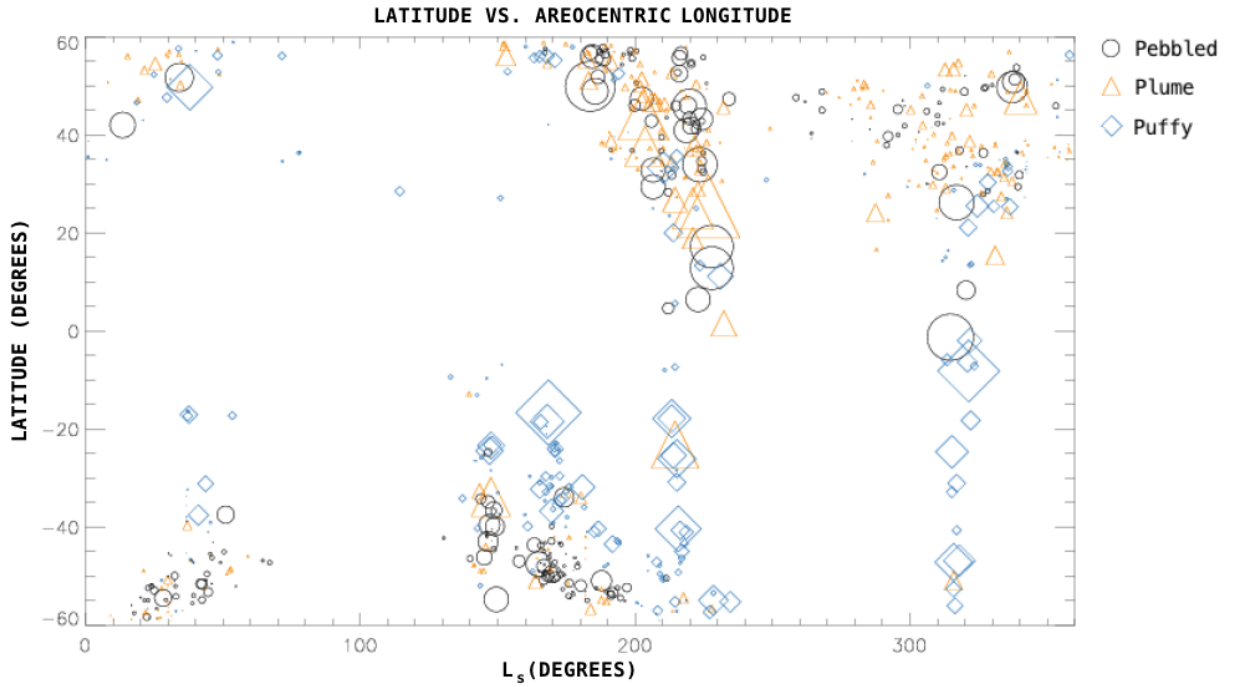


Figure 8. Latitudinal distribution of puffy, pebbled and plume morphologies as a function of areocentric longitude. The size of each symbol is proportional to the area of the lifting event.

This figure also highlights the different morphologies with colors. Pebbled and plume structures display a similar latitudinal distribution. They are concentrated at higher latitudes. In contrast, a significant portion of puffy structures also occur at lower latitudes. Figure 8 indicates that the largest lifting events with plume-like or pebbled structure tend to occur in the northern hemisphere and the largest puffy events tend to occur in the southern hemisphere. We find that 6.8 percent of pebbled, 8.4 percent of plume, and 21.8 percent of puffy events occur between 30° N/S.

Further research is needed to understand why pebbled and plume structures are mostly confined to higher latitudes while puffy structures also occur at lower latitudes. This may be related to the characteristics of the wind regime and planetary boundary layer (PBL) structures. Here we simply note that the wind stress associated with polar jets at high latitudes during the cold season is among the greatest over the planet and the surface temperature is warmer at lower latitudes than at higher latitudes.

5. Conclusion

We have used Mars Daily Global Maps (MDGMs) generated from the Mars Orbiter Camera (MOC) on board Mars Global Surveyor (MGS) from July of 1999 to January of 2005 (Mars Years 24–27), excluding the 2001 (Mars Year 25) global dust storm, to constructed a database of locations of active dust lifting. Using this database, we have analyzed dust lifting frequency, correlated frequency with surface wind stress and dust deposition rates simulated by models as well as surface properties derived from observations. We have assessed the seasonal and size distributions of lifting events, and studied the morphological features of lifting.

A definite seasonal pattern of dust lifting has been observed. Three seasonal windows have been identified in which lifting activity takes place: $L_s = 0^\circ\text{--}80^\circ$, $L_s = 130^\circ\text{--}230^\circ$, and $L_s = 260^\circ\text{--}360^\circ$. The average size of regions of active dust lifting varies with these seasonal windows. Small

scale lifting is more frequent than large scale lifting and that there is a rapid decay in the number of lifting events as surface area increases. Note this is not to say that small lifting area is more important. Apparently, major dust storms of global impact are associated with large lifting area. Events with large lifting areas tend to occur during the second seasonal window. This preference for small scale lifting and the severe trend of rapid decay in number of events as surface area increases also holds for each hemisphere. The number of lifting events in the north and the south are quite similar.

Several regions on Mars had high lifting frequencies. These included the Arcadia and Acidalia in the northern hemisphere and Hellas and Argyre in the southern hemisphere. Northern high frequency areas generally had low elevations, smooth topographies, and high surface wind stress [Basu *et al.*, 2006; Moholland *et al.*, 2013]. Lifting sites are more zonally uniform in the south. Inactive lifting regions included Tharsis, Arabia, and Elysium. These areas generally correspond to annual net dust deposition regions predicted by GCMs [Basu *et al.*, 2006].

We have presented a classification scheme for lifting morphologies. In this system, lifting events were defined to be puffy, pebbled, or plume structured. Our analysis shows that puffy, pebbled, and plume morphologies are apparent in each seasonal window. Although these structures show no seasonal difference, they do show a preference in latitudinal distribution. Pebbled and plume structures are concentrated at higher latitudes, while puffy lifting structures are found more often in low latitudes. Differences in wind speed and temperature may be related to this behavior. Further study is necessary to understand the observations reported in this paper.

Acknowledgments.

L. Kulowski is supported by the National Science Foundation Research Experiences for Undergraduates (REU) and Department of Defense ASSURE programs under NSF Grant no. 1262851 and by the Smithsonian Institution. H. Wang is supported by the NASA MDAP program.

References

- Basu, S., J. Wilson, M. Richardson, and A. Ingersoll (2006), "Simulation of spontaneous and variable global dust storms with the GFDL Mars GCM," *J. Geophys. Res.*, 111, doi: 10.1029/2005JE002660.
- Cantor, B. A. (2007), "MOC observations of the 2001 Mars planet-encircling dust storm," *Icarus*, 186, 60-96, doi: 10.1016/j.icarus.2006.08.019.
- Cantor, B. A., P. B. James, M. Caplinger, and M. J. Wolff (2001), "Martian dust storms: 1999 Mars Orbiter Camera observations," *J. Geophys. Res.*, 106, 23653-23688, doi: 10.1029/2000JE001310.
- Greeley, R., R. Leach, B. White, J. Iversen, and J. Pollock (1980), "Threshold wind speeds for sand on Mars: Wind tunnel simulations," *Geophys. Res Lett.*, 7(2), 121-124, doi: .
- Flaugergues, H. (1818), "Observations diverses de M. Flaugergues à Viviers," *Correspondance astronomique, géographique, hydrographique et statistique*, 1, 178-192.
- Hinson, D. P. and H. Wang (2010), "Further observations of regional dust storms and baroclinic eddies in the northern hemisphere of Mars," *Icarus*, 2006(1), 290-305, doi: 10.1016/j.icarus.2009.08.019.
- Liu, J., M. I. Richardson, and R. J. Wilson (2003), "An assessment of the global, seasonal, and interannual spacecraft record of Martian climate in the thermal infrared wind speeds for sand on Mars: Wind tunnel simulations," *J. Geophys. Res.*, 108(E8), 5089, doi: 10.1029/2002JE001921.
- Leovy, C. B., G. A. Briggs, A. T. Young, J. B. Pollack, E. N. Shipley, and R. L. Wildley (1972), "The martian atmosphere: Mariner 9 television experiment progress report," *Icarus*, 17 (2), 373-393.
- Martin, L. J. and R. W. Zurek (1993), "An analysis of the history of dust storm activity on Mars," *J. Geophys. Res.*, 100, 7509-7512, doi: 10.1029/92JE02937.
- Mulholland, D., P. Read, and S. Lewis, (2013), "Simulating the interannual variability of major dust storms on Mars using variable lifting thresholds," *Icarus*, 223, 344-358, doi: 10.1016/j.icarus.2012.12.003.
- Neubauer, F. M. (1966), "Thermal convection in the Martian atmosphere," *J. Geophys. Res.*, 71, 2156-2202, doi: 10.1029/JZ071i010p02419.
- Schiaparelli, G. (1895), "Alcune mutazioni importanti osservate nella superficie di Marte," *Astronomische Nachrichten*, 137, 97.
- Smith, M. (2008), "Spacecraft Observations of the Martian Atmosphere," *Annu. Rev. of Earth Planet. Sci.*, 36, 191-219, doi: 10.1146/annurev.earth.36.031207.124334.
- Strausberg, M., H. Wang, M. I. Richardson, S. P. Ewald, and A. D. Toigo (2005), "Observations of the initiation and evolution of the 2001 Mars global dust storm," *J. Geophys. Res.*, 110, doi: 10.1029/2004JE002361.
- Wang, H. (2007), "Dust storms originating in the northern hemisphere during the third mapping year of Mars Global Surveyor," *Icarus*, 189 (2), 325-343, doi: 10.1016/j.icarus.2007.01.014.
- Wang, H. and A. P. Ingersoll (2002), "Martian clouds observed by Mars Global Surveyor Mars Orbiter Camera," *J. Geophys. Res.*, 107, doi: 10.1029/2001JE001815.
- Wang, H. and M.I. Richardson (2013), "The origin, evolution and trajectory of large dust storms on Mars during Mars years 24-30," *Icarus*.